DOI: 10.1021/cg100245a

CRYSTAL GROWTH & DESIGN Article

2010, Vol. 10
2746–2751

A Series of Three-Dimensional 4d−4f Heterometallic Coordination Polymers with Six-Connected Doubly Interpenetrated pcu Net Topology: Structural, Photoluminescent, and Magnetic Properties

Zhao-Yang Li,[†] Jing-Wei Dai,[†] Ning Wang,[†] Hui-Hua Qiu,[‡] Shan-Tang Yue,*[,†] and Ying-Liang Liu*[,‡]

[†]*School of Chemistry & Environment, South China Normal University, Guangzhou, 510006, P. R. China, and* [‡]*Department of Chemistry, Jinan University, Guangzhou, P. R. China*

Received February 23, 2010; Revised Manuscript Received April 13, 2010

ABSTRACT: A series of lanthanide(III)-Ag(I) 4d−4f heterometallic coordination polymers (HCPs) with **pcu** topology, $\{[Ln^{III}\text{-}Ag^{I}(Hbidc)(bidc)(ox)_{0.5}(H_2O)]\cdot H_2O\}_n$ (Ln = Sm **1**, Eu **2**, Gd **3**, Tb **4**, Dy **5**, Ho **6**, Er **7**, H_2bidc = 1*H*-benzimidazole-5,6-dicarboxylic acid, ox = oxalate), have been synthesized through self-assembly reactions. All seven complexes are isostructural and have three-dimensional 2-fold interpenetrated structures, with both the organic ligand and oxalate groups acting as bridges. These new complexes crystallize with the same unique six-connected three-nodal net described by $(10^8\cdot12\cdot16^4\cdot18^2)$ $(10)_6$ topology. The ferromagnetic properties of complex **3** were investigated. Moreover, complexes **1**, **2**, **4**, and **5** exhibit very strong photoluminescence properties and with long lifetimes in the solid state at room temperature.

Introduction

Self-assembly processes directed by metal−ligand ligation have been extensively utilized to construct heterometallic coordination polymers (HCPs) with novel topologies and potentially interesting multifunctions in magnetism, photoluminescence, sorption, separation, catalysis, etc.[1,2] However, most of the works have so far focused on the assembly of the 3d−4f systems and the investigation of the interactions between 3d and 4f metal centers, especially lanthanide-copper(II) (Ln-Cu) and Ln-Mn HCPs.[3−8] But the construction of 4d−4f heterometallic multifunctional coordination polymers remains less developed.[9] From the synthetic point of view, the assembly of extended structures with high dimensionality lanthanide-transition metal heterometallic coordination frameworks is a formidable task because there are several complicated factors: (i) the choice of organic ligands; (ii) the control of the second ligand; and (iii) the competitive reaction between lanthanide and transition metal ions, etc.[10] Despite these factors, the selective strategy for main organic ligand containing appropriate coordination sites is crucial to construct target compounds. Therefore, the system composed of ligands containing N,O-donor atoms, such as pyrazinecarboxylic acid, pyridinecarboxylic acid, imidazolecarboxylic acid, can easily form heterometallic polymers.[11] Moreover, several types of inorganic ligands such as CN^-, N_3^-, Cl^-, Br^-, and I^- have also been used to construct heterometallic complexes.[12]

On the other hand, a variety of uninodal and binodal net topologies that are based on 3-, 4-, and 6-connected and boracite, pyrite, rutile, and Pt_3O_4 topologies have been realized.[13] However, owing to the limits of coordination numbers of metal centers and the steric hindrance issues of most commonly used organic ligands, it is still a great challenge to synthesize three-nodal six-connectivity interpenetrated 4d−4f HCPs.

On the basis of the above considerations, we chose 1*H*-benzimidazole-5,6-dicarboxylate (H_2bidc) as a potential linker between lanthanide and transition metal ions. H_2bidc is a semirigid and multidentate ligand that can afford up to six donor atoms (two N and four O atoms) with variable coordination modes. Under hydrothermal conditions, H_2bidc can be partially or fully deprotonated to generate $Hbidc^-$ and $bidc^{2-}$ anions at different pH values. Hence, it has a strong potential to construct highly ordered dimensional structures and becomes an excellent candidate for the construction of 4d−4f HCPs. Meanwhile, in our system we chose the "shorter" and "smart" organic ligand, $H_2C_2O_4$ (oxalate) as the second ligand, aiming to bridge the adjacent Ln ions, because the oxalate can play an important role in forming a zigzag chain or helical chain. As far as we know, three-dimensional Ln(III)-Ag(I) HCPs constructed from H_2bidc and oxalate as mixed ligands have not been reported.

Most of the previously reported high dimensional coordination polymers based on the H_2bidc ligand are composed of either d-block metals or single rare-earth metals,[14] while 3d−4f or 4d−4f heterometallic compounds with interpenetrated structures have not been reported in the literature. Zheng et al. reported the first single lanthanide-H_2bidc coordination polymer with 2D structures and Wu et al. obtained the single Mn(II)-H_2bidc complex with 3D supramolecular structure.[15,16] Ma et al. reported three new organotin polymers with H_2bidc and trimethyl chloride under different conditions.[17] Herein, we report the synthesis and characterizations of a series of lanthanide-transition metal 4d−4f complexes based on mixed organic ligands, namely, $\{[Ln^{III}Ag^{I}(Hbidc)(bidc)(ox)_{0.5}(H_2O)]\cdot H_2O\}_n$, which exhibit unprecedented six-connected doubly interpenetrated **pcu** net topology and show very strong photoluminescence properties (complexes **1**, **2**, **4**, and **5**) and ferromagnetic properties (complex **3**).

Experimental Section

Materials and Measurements. All chemicals employed were commercially available and used as received without further purificaion.

*To whom correspondence should be addressed. (S.T.Y.) E-mail: yuesht@scnu.edu.cn. Fax: +86-20-39310187. Tel: +86-20-39310187.

Published on Web 04/29/2010

Table 1. Crystal Data and Structure Refinement for $\{[Ln^{III}Ag^{I}(Hbidc)(bidc)(ox)_{0.5}(H_2O)]\cdot H_2O\}_n$

complex	1	2	3	4	5	6	7
empirical formula	$C_{19}H_{13}Ag-N_4SmO_{12}$	$C_{19}H_{13}Ag-N_4EuO_{12}$	$C_{19}H_{13}Ag-N_4GdO_{12}$	$C_{19}H_{13}Ag-N_4TbO_{12}$	$C_{19}H_{13}Ag-N_4DyO_{12}$	$C_{19}H_{13}Ag-N_4HoO_{12}$	$C_{19}H_{13}Ag-N_4ErO_{12}$
formula weight	747.56	749.17	754.45	756.13	759.7	762.13	764.46
T/K	298	173	298	298	298	298	298
crystal system	monoclinic	monoclinic	monoclinic	monoclinic	monoclinic	monoclinic	monoclinic
space group	$P2_1/c$	$P2_1/c$	$P2_1/c$	$P2_1/c$	$P2_1/c$	$P2_1/c$	$P2_1/c$
a /Å	6.7947(12)	6.7488(5)	6.7830(8)	6.7737(4)	6.7179(8)	6.7583(6)	6.7425(15)
b /Å	15.969(3)	15.9140(11)	15.9415(18)	15.9327(10)	15.8721(18)	15.9101(15)	15.880(4)
c /Å	19.395(4)	19.3628(13)	19.364(2)	19.3375(12)	19.303(2)	19.3168(18)	19.277(4)
α	90	90	90	90	90	90	90
β /°	92.970(3)	92.7970(10)	92.669(2)	92.4080(10)	92.1960(10)	92.0030(10)	91.797(3)
γ /°	90	90	90	90	90	90	90
V /Å^3	2106.6(7)	2077.1(3)	2091.6(4)	2085.1(2)	2056.8(4)	2075.8(3)	2062.9(8)
Z	4	4	4	4	4	4	4
D_c/g cm^3	2.363	2.396	2.396	2.409	2.454	2.439	2.461
μ/mm^{-1}	3.779	4.016	4.160	4.384	4.639	4.809	5.071
F(000)	1440.0	1444.0	1448.0	1452.0	1456.0	1460.0	1464.0
reflections collected/unique	10663/4006	11792/4400	9384/4056	8622/4066	11016/4007	11022/4044	10774/3965
GOF	1.067	1.014	1.002	1.023	1.021	1.037	1.082
$R_1{}^a/wR_2{}^b$ [$I > 2\sigma(I)$]	0.0630/0.1490	0.0246/0/0552	0.0356/0.0706	0.0281/0.0574	0.0300/0.0610	0.0213/0.0457	0.0512/0.1068
R_1/wR_2 (all data)	0.0918/0.1675	0.0291/0.0572	0.0545/0.0778	0.0386/0.0618	0.0406/0.0649	0.0272/0.0481	0.0683/0.1141
CCDC number	745826	726063	745827	726065	726064	745828	726066

$^a R_1 = \sum||F_0| - |F_c||/\sum|F_0|$. $^b wR_2 = \{\sum[w(F_0^2 - F_c^2)^2]/\sum(wF_0^2)^2\}^{1/2}$.

The C, H, and N microanalyses were carried out with a Perkin-Elmer 240 elemental analyzer. The FT-IR spectra were recorded from KBr pellets in the 4000−400 cm^{-1} ranges on a Nicolet 5DX spectrometer. Thermogravimetric analyses were performed on Perkin-Elmer TGA7 analyzer with a heating rate of 10 °C/min in flowing air atmosphere. Fluorescence spectroscopy data were recorded on an Edinburgh F900 FLS-900 spectrophotometer analyzer with a xenon arc lamp as the light source. In the measurements of emission and excitation spectra, the pass width is 5.0 nm. The magnetic susceptibility data were collected from polycrystalline samples at an external field of 1 T on a MPMS XL-7 magnetometer (Quantum Design) in the temperature range 2−300 K. The output data were corrected for the diamagnetism of the sample holder and of the samples calculated from their Pascal constants. Powder X-ray diffraction (PXRD) patterns were recorded on a X-pert diffractometer or Rigaku D/M-2200T automated diffractometer for Cu Kα radiation (λ = 1.54056 Å), with a scan speed of 4° min^{-1} and a step size of 0.02° in 2θ range of 5−50°.

Syntheses. A mixture of 1*H*-benzimidazole-5,6-dicarboxylic acid (0.1037 g, 0.5 mmol), $H_2C_2O_4$ (0.0378 g, 0.3 mmol), $Sm(NO_3)_3\cdot 6H_2O$ for **1** (0.135 g, 0.3 mmol), $Eu(NO_3)_3\cdot 6H_2O$ for **2** (0.135 g, 0.3 mmol), $Gd(NO_3)_3\cdot 6H_2O$ for **3** (0.135 g, 0.3 mmol), $Tb(NO_3)_3\cdot 6H_2O$ for **4** (0.135 g, 0.3 mmol), $Dy(NO_3)_3\cdot 6H_2O$ for **5** (0.135 g, 0.3 mmol), $Ho(NO_3)_3\cdot 6H_2O$ for **6** (0.135 g, 0.3 mmol), $Er(NO_3)_3\cdot 6H_2O$ for **7** (0.135 g, 0.3 mmol), $AgNO_3$ (0.051 g, 0.3 mmol), and H_2O (10 mL) was heated to 160 °C for 72 h in a 23 mL Teflon-lined stainless-steel autoclave and then cooled to room temperature at a rate of 5 °C/h. Colorless prismatic crystals were collected and dried in air.

$\{[Sm^{III}Ag^{I}(Hbidc)(bidc)(ox)_{0.5}(H_2O)]\cdot H_2O\}_n$ **(1).** Yield: 75% based on Sm. Anal. Calcd for $C_{19}H_{13}AgN_4SmO_{12}$: C, 30.37; H, 1.64; N, 7.52%. Found: C, 30.50; H, 1.74; N, 7.49%. IR frequencies (KBr, cm^{-1}, Figure S3, Supporting Information).

$\{[Eu^{III}Ag^{I}(Hbidc)(bidc)(ox)_{0.5}(H_2O)]\cdot H_2O\}_n$ **(2).** Yield: 80% based on Eu. Anal. Calcd for $C_{19}H_{13}AgN_4EuO_{12}$: C, 30.38; H, 1.74; N, 7.54%. Found: C, 30.43; H, 1.73; N, 7.47%. IR frequencies (KBr, cm^{-1}, Figure S4, Supporting Information).

$\{[Gd^{III}Ag^{I}(Hbidc)(bidc)(ox)_{0.5}(H_2O)]\cdot H_2O\}_n$ **(3).** Yield: 78% based on Gd. Anal. Calcd for $C_{19}H_{13}AgN_4GdO_{12}$: C, 30.27; H, 1.74; N, 7.58%. Found: C, 30.22; H, 1.72; N, 7.42%. IR frequencies (KBr, cm^{-1}, Figure S5, Supporting Information).

$\{[Tb^{III}Ag^{I}(Hbidc)(bidc)(ox)_{0.5}(H_2O)]\cdot H_2O\}_n$ **(4).** Yield: 75% based on Tb. Anal. Calcd for $C_{19}H_{13}AgN_4TbO_{12}$: C, 30.22; H, 1.64; N, 7.49%. Found: C, 30.15; H, 1.72; N, 7.41%. IR frequencies (KBr, cm^{-1}, Figure S6, Supporting Information).

$\{[Dy^{III}Ag^{I}(Hbidc)(bidc)(ox)_{0.5}(H_2O)]\cdot H_2O\}_n$ **(5).** Yield: 79% based on Dy. Anal. Calcd for $C_{19}H_{13}AgN_4DyO_{12}$: C, 30.07; H, 1.59; N, 7.32%. Found: C, 30.01; H, 1.71; N, 7.37%. IR frequencies (KBr, cm^{-1}, Figure S7, Supporting Information).

$\{[Ho^{III}Ag^{I}(Hbidc)(bidc)(ox)_{0.5}(H_2O)]\cdot H_2O\}_n$ **(6).** Yield: 76% based on Ho. Anal. Calcd for $C_{19}H_{13}AgN_4HoO_{12}$: C, 30.01; H, 1.61; N, 7.29%. Found: C, 29.92; H, 1.71; N, 7.35%. IR frequencies (KBr, cm^{-1}, Figure S8, Supporting Information).

$\{[Er^{III}Ag^{I}(Hbidc)(bidc)(ox)_{0.5}(H_2O)]\cdot H_2O\}_n$ **(7).** Yield: 70% based on Er. Anal. Calcd for $C_{19}H_{13}AgN_4ErO_{12}$: C, 29.92; H, 1.58; N, 7.32%. Found: C, 29.82; H, 1.70; N, 7.33%. IR frequencies (KBr, cm^{-1}, Figure S9, Supporting Information).

X-ray Crystallographic Measurements. Data collections were performed at 298 K on a Bruker Smart Apex II diffractometer with graphite-monochromated Mo Kα radiation (λ = 0.71073 Å) for complexes **1**−**7**. Absorption corrections were applied by using the multiscan program SADABS. Structural solutions and full-matrix least-squares refinements based on F^2 were performed with the SHELXS-97 and SHELXL-97 program packages, respectively.[19] All the non-hydrogen atoms were refined anisotropically. The organic hydrogen atoms were generated geometrically (C−H = 0.93 or 0.96 Å), and the water hydrogen atoms were located from difference maps and refined with isotropic temperature factors. Details of the crystal parameters, data collections, and refinement for complexes **1**−**7** are summarized in Table 1. Hydrogen-bonding data for complex **5** are listed in Table S1, Supporting Information.

Results and Discussion

Synthesis and Crystal Structures. The colorless crystals of **1**−**7** were obtained in good yield by the one-pot hydrothermal reactions of $Ln(NO_3)_3\cdot 6H_2O$, $AgNO_3$, H_2bidc, and H_2ox. These polymers crystallize in space group $P2_1/c$ and all of them are isostructural. Herein, only the structure of complex **1** is described in detail.

An *ORTEP* view of **1** is shown in Figure 1; the asymmetric unit of **1** contains one Sm(III) ion, two one-half Ag(I) ions which are lying about the inversion center, two independent H_2bidc ligands, one-half oxalate ligand which lies about an inversion center, and one coordinated water molecule and one lattice water molecule. The central Sm(III) atom is nine-coordinated in a distorted tricapped trigonal prismatic geometry with six oxygen atoms from the bidc^{2-} and Hbidc$^-$ ligands, two O atoms from the oxalate ligands, and one O atom from the coordinated water molecule, respectively. The two-coordinated Ag(I) ion exhibits linear coordination

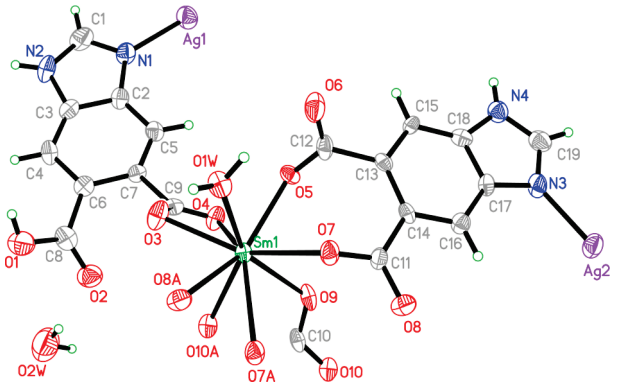

Figure 1. *ORTEP* view of the unit cell of **1** (50% thermal ellipsoids).

Scheme 1. Two New Coordination Modes of H_2bidc Ligand

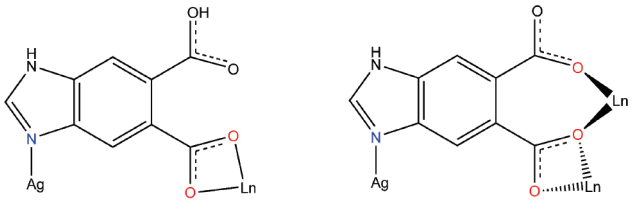

geometry [the angles of N−Ag(1)−N, N−Ag(2)−N are close to 180°]. The Sm−O bond distances range from 2.322(7) to 2.710(7) Å. The bond angles of O−Sm−O are in the range of 50.2(2)−151.4(3)°. In this structure, the H_2bidc ligand exhibits two kinds of unreported coordination modes, mode **a**: the nitrogen atom coordinates to the silver center and the 6-carboxylate oxygen atoms chelate the Sm(III) center with the μ_2-(κ^3 N^3, O^6: O^6)-bridging mode; mode **b**: the nitrogen atom coordinates to the silver center, while one of the 5-carboxylate oxygen atoms and the 6-carboxylate coordinate to two samarium centers with the μ_3-(κ^5 N^3, O^5: O^6: O^6: O^6)-bridging mode (Scheme 1). The carboxyl groups of organic ligands are not fully deprotonated, in agreement with the IR analysis that the absorption peaks around 1700 cm^{-1} are observed.

The oxalate dianion behaves as a μ-κ^4 O bridge, connecting the adjacent Sm(III) ions into a zigzag chain and the distances between Sm(III) ions are 4.2445(10) and 6.2157(11) Å (Figure 2a). The 1D motifs are further extended by Ag(bidc)$_2$ to result in a 2D pillar-chain structure, and the distance between the adjacent Ag(I) is 6.7947(12) Å (Figure 2b). Notably, the 2D layer structure can also be viewed as gear wheel secondary building unit (SBU) (Figure S1, Supporting Information) which is linked by the Ag(I) ion to give rise to a 3D framework (Figure 3). It is of interest that the dinuclear Sm centers can be seen as the six-connected node, and the two-coordinated Ag(I) center is serving as the ditopic linker. The linking mode of L−Ag−L can be regarded as the four-connected bridge, and the oxalate ligands are the other bridges. Therefore, the whole network is doubly interpenetrated six-connected **pcu** network (Figure 4). Meanwhile, topological studies performed using the software package TOPOS 4.0[18] reveal that this topology is a unique three-nodal six-connected net, as confirmed by TOPOS 4.0 in conjunction with systematic searches in the literature. Its Schläfli symbol is $(10^8 \cdot 12 \cdot 16^4 \cdot 18^2)$ $(10)_6$. To the best of our knowledge, this is the first reported example of a 3D heterometallic six-connected network with 2-fold interpenetrated structures.

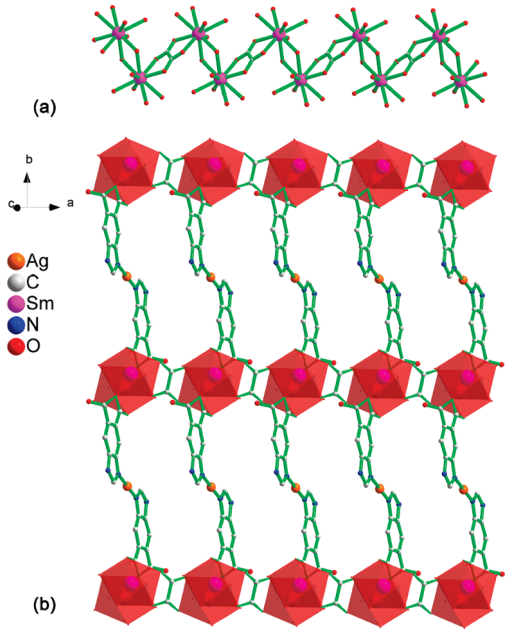

Figure 2. (a) 1D lanthanide chain connected by the oxalate ligand. (b) Two-dimensional layer structure constructed by 1D chain and Ag(bidc)$_2$ unit.

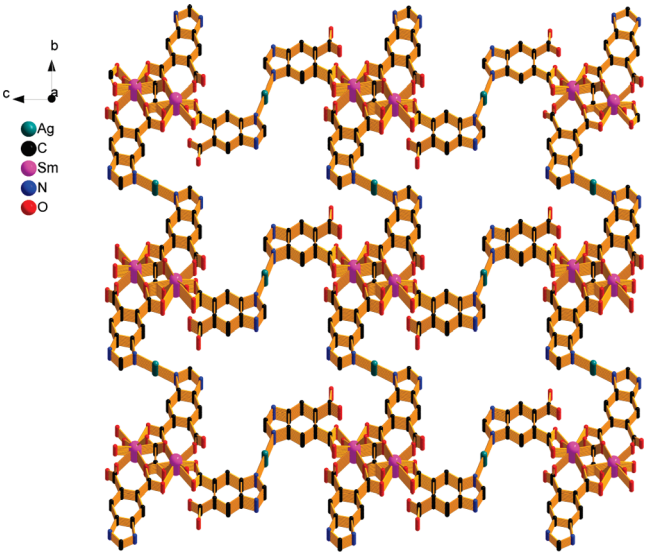

Figure 3. View of 3D framework for **1** based on the linkage of adjacent 2D gear wheel subunits.

Thermal Stability, IR and PXRD Analysis. The TGA of complexes **3**−**7** were performed in air atmosphere from 50 to 800 °C at a heating rate of 10 °C/min, as can be seen in Figure S2, Supporting Information. These complexes undergo two steps of weight loss and can be stable up to about 330 °C. The free water molecule and coordinated water molecules were gradually lost in the temperature range of 80−300 °C, and a weight loss of approximate 5.4% was observed (calculated 4.8%). The consecutive weight loss from 330 to 450 °C is probably caused by the decomposition of the H_2bidc ligands and the oxalate, resulting in the collapse of frameworks.

The IR spectra of **1**−**7** are similar (Figures S3−S9, Supporting Information). The strong and broad absorption bands in the range of 3050−3500 cm^{-1} in **1**−**7** are ascribed to the characteristic vibration of OH^-. The strong vibrations

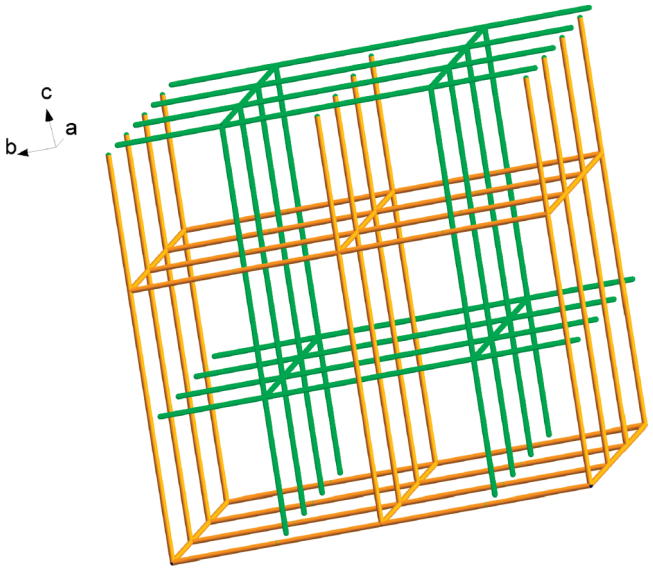

Figure 4. Six-connected 2-fold interpenetrated **pcu** net topology (L−Ag−L as the ditopic linker, dinuclear Sm atom as the six-connected node, the organic ligand as the connected bridge).

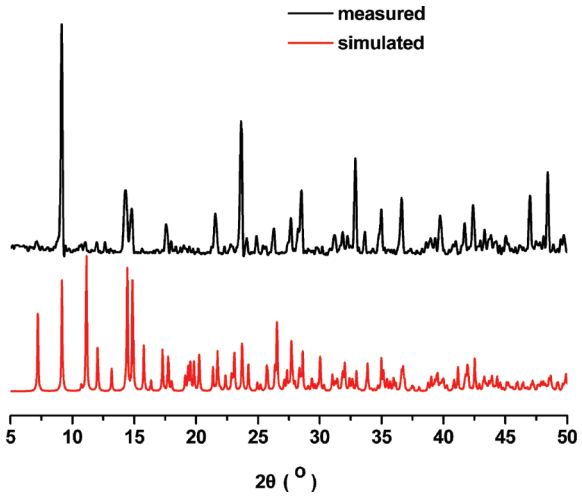

Figure 5. (Top) The experimental PXRD pattern of complex **5** at room temperature.
(Bottom) The simulated PXRD pattern from single crystal X-ray data of complex **5**.

appearing around 1590 and 1410 cm^{-1} correspond to the asymmetric and symmetric stretching vibrations of the carboxylate groups, respectively. The middle strong bands around 1700 cm^{-1} indicate that the organic ligands are not fully deprotonated. The strong bands in the range of 1590−1690 cm^{-1} in all these complexes imply the C=C and C=N stretching bands of imidazole ring in the H_2bidc ligand.

The as-isolated samples of the selected five complexes were also characterized by powder X-ray diffraction at room temperature (Figures 5 and S10−S13). When compared to the simulated patterns based on the single crystal data samples, the experimental patterns are in agreement with the calculated diffractograms, thus basically pointing toward the formation of only a single phase product under the reaction conditions employed for these complexes.

Photoluminescent Properties. Because of the excellent luminescent properties of Sm(III), Eu(III), Tb(III), and Dy(III) ions,

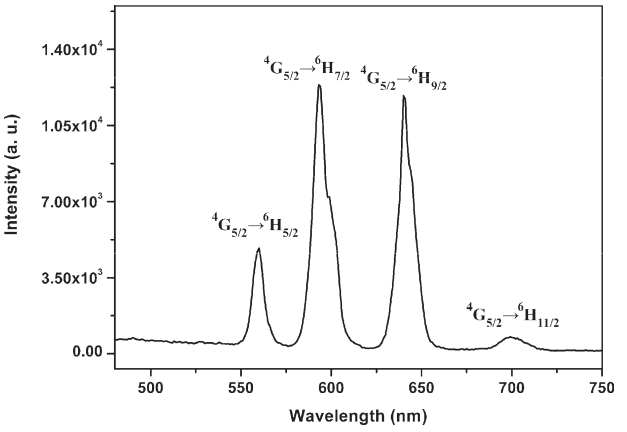

Figure 6. Solid-state emission spectrum for **1** in the solid state at room temperature (excited at 307 nm).

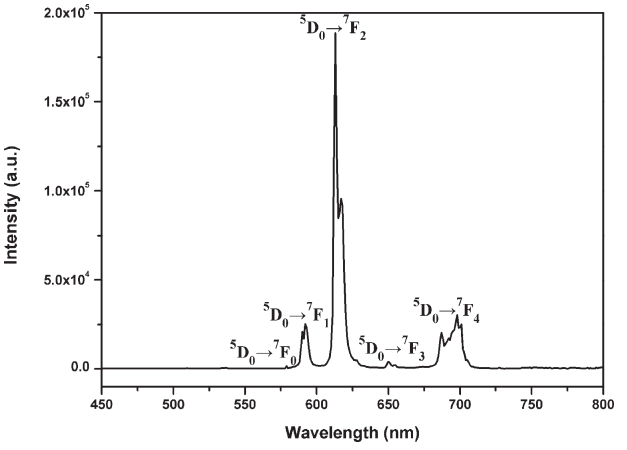

Figure 7. Solid-state emission spectrum for **2** in the solid state at room temperature (excited at 395 nm).

the photoluminescence of complexes **1**, **2**, **4**, and **5** and their lifetimes were investigated in the solid state at room temperature. In the emission spectra of **1** (Figure 6), four peaks at 560, 594, 640, and 699 nm correspond to $^4G_{5/2} \rightarrow {}^6H_{5/2}$, $^4G_{5/2} \rightarrow {}^6H_{7/2}$, $^4G_{5/2} \rightarrow {}^6H_{9/2}$, and $^4G_{5/2} \rightarrow {}^6H_{11/2}$ transitions of the Sm(III) ion. As shown in Figure 7, the emission spectra of **2** upon excitation at 395 nm displays intense red luminescence and exhibits the characteristic transitions of $^5D_0 \rightarrow {}^7F_n$ ($n = 0 \rightarrow 4$) of Eu(III) ions at 580, 592, 616, 652, and 698 nm, respectively. The band at 616 nm can be attributed to electric-dipolar $^5D_0 \rightarrow {}^7F_2$ transition, the band at 592 nm can be assigned to magnetic-dipolar $^5D_0 \rightarrow {}^7F_1$. The intensity of the $^5D_0 \rightarrow {}^7F_2$ transition is stronger than that of the $^5D_0 \rightarrow {}^7F_1$ transition with the intensity ratio $I(^5D_0 \rightarrow {}^7F_2)/I(^5D_0 \rightarrow {}^7F_1)$ of ca. 7.5, indicating that Eu(III) ions have a low symmetric coordination environment and without an inversion center, which is confirmed by the X-ray crystal structure of **2**. In addition, ligand to silver(I) energy transfer is invisible, which is testified by the fact that no other emission peaks exist in the spectra except the characteristic emission peaks of Eu(III) ions. The luminescent spectrum of **4** is shown in Figure 8. The bands at 489, 543, 587, 621, and 652 nm can be attributed to the $^5D_4 \rightarrow {}^7F_6$, $^5D_4 \rightarrow {}^7F_5$, $^5D_4 \rightarrow {}^7F_4$, $^5D_4 \rightarrow {}^7F_3$ and $^5D_4 \rightarrow {}^7F_2$ transitions, respectively, where the peak at 545 nm is the strongest one. Complex **5** displays yellow photoluminescent behavior with typical Dy(III) emissions at 477, 572, and 661 nm (Figure 9) corresponding to the characteristic emission $^4F_{2/9} \rightarrow {}^6H_J$ transitions of Dy(III) ion

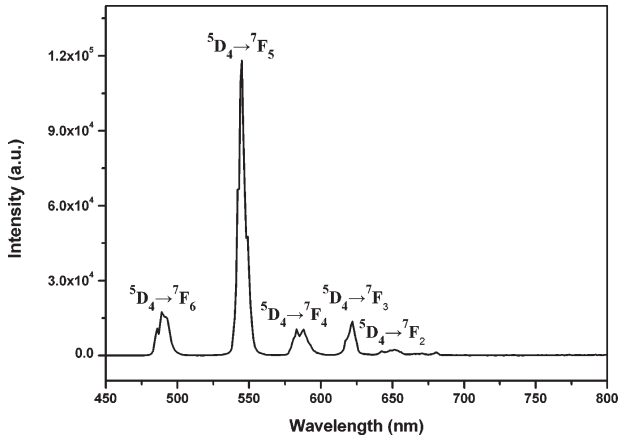

Figure 8. Solid-state emission spectrum for **4** in the solid state at room temperature (excited at 308 nm).

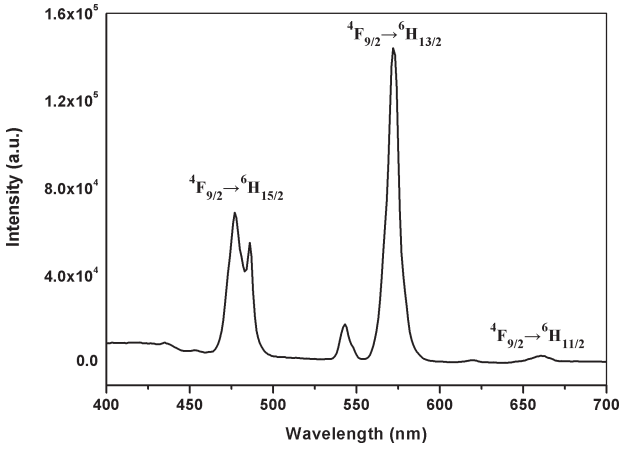

Figure 9. Solid-state emission spectrum for **5** in the solid state at room temperature (excited at 302 nm).

($J = 15/2, 13/2, 11/2$). The yellow emission of the $^4F_{2/9} \rightarrow {}^6H_{13/2}$ transition has a stronger intensity than the blue emission of $^4F_{2/9} \rightarrow {}^6H_{15/2}$ for complex **5**. From the photoluminescent properties of compounds mentioned above, it can be seen that, under excitation of UV rays, the emissions of solid samples containing Sm(III)−Ag(I), Eu(III)−Ag(I), Tb(III)−Ag(I), and Dy(III)−Ag(I) ions have all been efficiently sensitized by the mixed organic ligands in the visible region at room temperature and exhibit the characteristic transition of the Sm(III), Eu(III), Tb(III), and Dy(III) ions, respectively.

The luminescence decay curves of complexes **1**, **2**, **4** and **5** were measured at room temperature. The decay curves are well fitted into a single-exponential function as $I = I_0 \exp(-t/\tau)$, indicating the existence of a single chemical environment of Ln(III) sites in the structure.[20] The corresponding lifetime for complex **2** is about 0.2721 ms, whereas that for complex **4** is about 0.4876 ms (determined by monitoring the $^5D_0 \rightarrow {}^7F_2$ line and the $^5D_4 \rightarrow {}^7F_5$ line, respectively, Figures S14−S15, Supporting Information). Both of them have long luminescence lifetimes at millisecond order, which are comparable to other corresponding Eu(III) and Tb(III) complexes.[21] The lifetimes of complexes **1** and **5** are about 3.626 and 2.460 μs, respectively, which are much shorter than that for complexes **2** and **4** (Figures S16−S17, Supporting Information). Because the excitation falls in the range of those commercially available, complexes **2** and **4** can be good candidates for light-emitting diodes (LEDs) and other light applications.

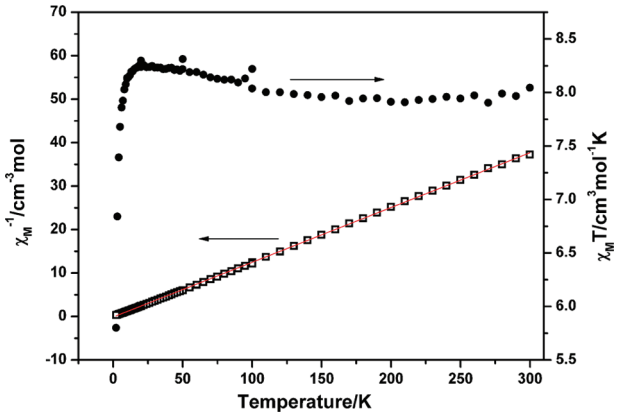

Figure 10. Thermal dependence of the $\chi_M T$ and $\chi_M{}^{-1}$ curves at $H = 1$ T. The red line represents the best fit.

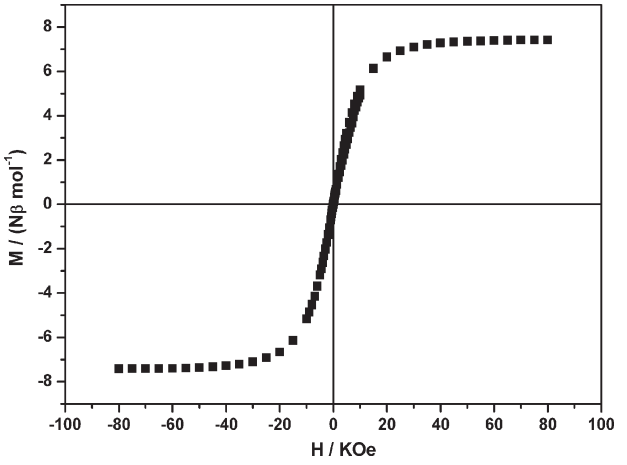

Figure 11. The hysteresis loop of complex **3** at 2 K.

Magnetic Property. The solid-state direct-current magnetic susceptibility measurement of **3** was performed in the range of 2−300 K under a field of 1 T, and the magnetic behavior is shown in Figure 10, as plots of $\chi_M T$ versus T and $\chi_M{}^{-1}$ versus T, where χ_M is the molar magnetic susceptibility for complex **3**. The room-temperature $\chi_M T$ value ($T = 300$ K) is 8.05 cm^3 mol^{-1} K, larger than the predicted spin-only value, 7.88 cm^3 mol^{-1} K for the unit of complex **3** composed of one paramagnetic Gd(III) ion and one diamagnetic Ag(I) ion. In the range of 15−300 K, as the temperature was lowered, the $\chi_M T$ value was continuously increased from 8.05 cm^3 mol^{-1} K to 8.22 cm^3 mol^{-1} K, which may be ascribed to the ferromagnetic interactions between Gd(III) ions. However, below 15 K, there is an abrupt $\chi_M T$ drop, which may be attributed to the saturated magnetization. In the range of 2−300 K, the $\chi_M{}^{-1}$ value obeys the Curie−Weiss law, $\chi = C/(T - \theta)$ with $C = 7.94$ cm^3 mol^{-1} K, $\theta = 0.82$ K.

Further magnetic characterization of **3** was performed by field-dependent magnetization at $T = 2$ K in the applied magnetic field range 0−8 T. Figure 11 shows that the isotherm magnetization experiences a rapid increase in $M - H$ at the start of the lower field, followed by a smooth increase in the saturation magnetization at $H = 6$ T. The $Ms = 7.41\ N\beta$ is slightly larger than $7\ N\beta$, expected for each Gd(III) unit. A sigmoidal-shaped hysteresis loop is provided, indicating the soft ferromagnetic behavior because of nondetectable coercivity in **3**.

Conclusion

In summary, we have synthesized and structurally characterized seven novel three-dimensional 4d−4f multifunctional HCPs with unusual six-connected three-nodal 2-fold interpenetrated **pcu** topology. The title complexes are the first examples of hybrid materials derived from the H_2bidc ligand. The Sm(III), Eu(III), Tb(III), and Dy(III) complexes display intense luminescence properties with efficient ligand-to-metal energy transfer, suggesting that these compounds have great potential applications as luminescent materials. Moreover, complex **3** exhibits weak ferromagnetic interactions between Gd(III) ions. This successful synthetic idea can be used to prepare other novel high-dimensional lanthanide-transition metal heterometallic hybrid materials with particular polyfunctions. In addition, although the present materials do not possess permanent porosity, the functionalized H_2bidc ligand have been used to construct porous materials with multifunctions by us. Further studies along this line are underway.

Acknowledgment. This work was financially supported by Guangdong Provincial Science and Technology Bureau (Grant 2008B010600009), and NSFC (Grant Nos. 20971047 and U0734005).

Supporting Information Available: 2D layer structure; TG curves of **3**−**7**; IR spectra of **1**−**7**; powder X-ray diffraction data of **2**, **3**, **6**, and **7**; PL decay curves; table of hydrogen bonds for **5**. Crystallographic information files. This material is available free of charge via the Internet at http://pubs.acs.org.

References

(1) (a) Zaworotko, M. J. *Chem. Soc. Rev.* **1994**, 283. (b) Yaghi, O. M.; Li, H.-L.; Davis, C.; Richardson, D.; Groy, T. L. *Acc. Chem. Res.* **1998**, *31*, 474. (c) Batten, S. R.; Robson, R. *Angew. Chem., Int. Ed.* **1998**, *37*, 1460. (d) Fujita, M.; Kwon, Y. J.; Washizu, S.; Ogura, K. *J. Am. Chem. Soc.* **1994**, *116*, 1151. (e) Gardner, G. B.; Venkataraman, D.; Moore, J. S.; Lee, S. *Nature* **1995**, *374*, 792. (f) Kim, H.; Samsonenko, D. G.; Das, S.; Kim, G. H.; Lee, H. S.; Dybtsev, D. N.; Berdonosova, E. A.; Kim, K. *Chem. Asian J.* **2009**, *4*, 886. (g) Wu, D.-Y.; Sato, O.; Einaga, Y.; Duan, C.-Y. *Angew. Chem., Int. Ed.* **2009**, *48*, 1475. (h) Takahashi, K.; Cui, H.-B.; Okano, Y.; Kobayashi, H.; Mori, H.; Tajima, H.; Einaga, Y.; Sato, O. *J. Am. Chem. Soc.* **2008**, *130*, 6688.

(2) (a) Min, K. S.; Suh, M. P. *J. Am. Chem. Soc.* **2000**, *122*, 6834. (b) Kondo, S.; Kitagawa, M.; Seki, K. *Angew. Chem., Int. Ed.* **2000**, *39*, 2081. (c) Eddaoudi, M.; Moler, D. B.; Li, H.-L.; Chen, B.-L.; Reineke, T. M.; O'Keeffe, M.; Yaghi, O. M. *Acc. Chem. Res.* **2001**, *34*, 319. (d) Rebilly, J. N.; Bacsa, J.; Rosseinsky, M. J. *Chem. Asian J.* **2009**, *4*, 892. (e) Ghosh, S. K.; Azhakar, R.; Kitagawa, S. *Chem. Asian J.* **2009**, *4*, 870. (f) Juhsz, G.; Matsuda, R.; Kanegawa, S.; Inoue, K.; Sato, O.; Yoshizawa, K. *J. Am. Chem. Soc.* **2009**, *131*, 4560. (g) Sato, O.; Tao, J.; Zhang, Y.-Z. *Angew. Chem., Int. Ed.* **2007**, *46*, 2152. (h) Li, G.-M.; Akitsu, T.; Einaga, Y. *J. Am. Chem. Soc.* **2003**, *125*, 12396.

(3) (a) Wang, N.; Yue, S.-T.; Liu, Y.-L.; Yang, H.-Y.; Wu, H.-Y. *Cryst. Growth Des.* **2009**, *9*, 368. (b) Xiang, S.-C.; Hu, S.-M.; Sheng, T.-L.; Chen, J.-S.; Wu, X.-T. *Chem.−Eur. J.* **2009**, *15*, 12496. (c) Stamatatos, T. C.; Teat, S. J.; Wernsdorfer, W.; Christou, G. *Angew. Chem., Int. Ed.* **2009**, *48*, 521.

(4) (a) Shutaro, O.; Takafumi, K.; Naohide, M.; Nazzareno, R.; Andrzej, P.; Jerzy, M. *J. Am. Chem. Soc.* **2004**, *126*, 420. (b) Mereacre, V.; Ako, A. M.; Clérac, R.; Wernsdorfer, W.; Hewitt, I. J.; Anson, C. E.; Powell, A. K. *Chem.−Eur. J.* **2008**, *14*, 3677. (c) Luo, F.; Batten, S. R.; Che, Y.-X.; Zheng, J.-M. *Chem.−Eur. J.* **2007**, *13*, 4948.

(5) (a) Valeriu, M. M.; Ayuk, M. A.; Rodolphe, C.; Wolfgang, W.; George, F.; Juan, B.; Christopher, E. A.; Annie, K. P. *J. Am. Chem. Soc.* **2007**, *129*, 9248. (b) Pointillart, F.; Bernot, K.; Sessoli, R.; Gatteschi, D. *Chem.−Eur. J.* **2007**, *13*, 1602.

(6) (a) Zaleski, C.; Depperman, E.; Kampf, J.; Kirk, M.; Pecoraro, V. *Angew. Chem., Int. Ed.* **2004**, *43*, 3912. (b) Mishra, A.; Wernsdorfer, W.; Abboud, K.; Christou, G. *J. Am. Chem. Soc.* **2004**, *126*, 15648. (c) Mishra, A.; Wernsdorfer, W.; Parson, S.; Christou, G.; Brechin, E. *Chem. Commun.* **2005**, 2086.

(7) (a) Sun, Y.-Q.; Zhang, J.; Yang, G.-Y. *Chem. Commun.* **2006**, 4700. (b) Figuerola, A.; Ribas, J.; Solans, X.; Font-Bardía, M.; Maestro, M.; Diaz, C. *Eur. J. Inorg. Chem.* **2006**, *9*, 1846.

(8) (a) Li, Z.-Y.; Wang, N.; Dai, J.-W.; Yue, S.-T.; Liu, Y.-L. *CrystEngComm* **2009**, *11*, 2003. (b) Chi, Y.-X.; Niu, S.-Y.; Wang, Z.-L.; Jin, J. *Eur. J. Inorg. Chem.* **2008**, *11*, 2336.

(9) (a) Gu, X.-J.; Xue, D.-F. *Cryst. Growth Des.* **2006**, *6*, 2551. (b) Lian, Q.-Y.; Huang, C.-D.; Zeng, R.-H.; Qiu, Y.-C.; Mou, J.-X.; Deng, H.; Zeller, M. *Z. Anorg. Allg. Chem.* **2009**, *635*, 393. (c) Gu, X.-J.; Xue, D.-F. *Cryst. Growth Des.* **2007**, *7*, 1726. (d) Mou, J.-X.; Zeng, R.-H.; Qiu, Y.-C.; Zhang, W.-G.; Deng, H.; Zeller, M. *Inorg. Chem. Commun.* **2008**, *11*, 1347.

(10) Huang, Y.-G.; Jiang, F.-L.; Hong, M.-C. *Coord. Chem. Rev.* **2009**, *253*, 2814.

(11) (a) Lin, X.-M.; Ying, Y.; Chen, L.; Fang, H.-C.; Zhou, Z.-Y.; Zhan, Q.-G.; Cai, Y.-P. *Inorg. Chem. Commun.* **2009**, *12*, 316. (b) Zhang, Q.; Zheng, Y.-X.; Liu, C.-X.; Sun, Y.-G.; Gao, E.-J. *Inorg. Chem. Commun.* **2009**, *12*, 523. (c) Sun, Y.-G.; Yan, X.-M.; Ding, F.; Gao, E.-J.; Zhang, W.-Z.; Verpoort, F. *Inorg. Chem. Commun.* **2008**, *11*, 1117. (d) Liu, Z.-H.; Qiu, Y.-C.; Li, Y.-H.; Deng, H.; Zeller, M. *Polyhedron* **2008**, *27*, 3493. (e) Gu, X.-J.; Xue, D.-F. *CrystEngComm.* **2007**, *6*, 471. (f) Cai, Y.-P.; Yu, Q.-Y.; Zhou, Z.-Y.; Hu, Z.-J.; Fang, H.-C.; Wang, N.; Zhan, Q.-G.; Chen, L.; Su, C.-Y. *CrystEngComm.* **2009**, *6*, 1006.

(12) (a) Yang, Y.-T.; Luo, F.; Che, Y.-X.; Zheng, J.-M. *Cryst. Growth Des.* **2008**, *8*, 3508. (b) Cheng, J.-W.; Zheng, S.-T.; Ma, E.; Yang, G.-Y. *Inorg. Chem.* **2007**, *46*, 10534. (c) Cheng, J.-W.; Zheng, S.-T.; Yang, G.-Y. *Inorg. Chem.* **2007**, *46*, 10261. (d) Gu, X.-J.; Xue, D.-F. *Inorg. Chem.* **2007**, *46*, 5349.

(13) (a) Blake, A. J.; Champness, N. R.; Hubberstey, P.; Li, W.-S.; Withersby, M. A.; Schroder, M. *Coord. Chem. Rev.* **1999**, *183*, 117. (b) Real, J. A.; Andres, E.; Munoz, M. C.; Julve, M.; Granier, T.; Bousseksou, A.; Varret, F. *Science* **1995**, *268*, 265. (c) Batten, S. R.; Hoskins, B. F.; Robson, R. *Chem.−Eur. J.* **2000**, *6*, 156. (d) Carlucci, L.; Cozzi, N.; Ciani, G.; Moret, M.; Proserpio, D. M.; Rizzato, S. *Chem. Commun.* **2002**, 1354. (e) Gudbjartson, H.; Biradha, K.; Poirier, K. M.; Zaworotko, M. J. *J. Am. Chem. Soc.* **1999**, *121*, 2599. (f) Keller, S. W.; Lopez, S. *J. Am. Chem. Soc.* **1999**, *121*, 6306. (g) Noro, S. I.; Kitagawa, S.; Kondo, M.; Seki, K. *Angew. Chem., Int. Ed.* **2000**, *39*, 2081. (h) Moulton, B.; Lu, J.; Zaworotko, M. J. *J. Am. Chem. Soc.* **2001**, *123*, 9224.

(14) (a) Lo, Y.-L.; Wang, W.-C.; Lee, G.-A.; Liu, Y.-H. *Acta Crystallogr., Sect. E* **2007**, *63*, m2657. (b) Gao, Q.; Gao, W.-H.; Zhang, C.-Y.; Xie, Y.-B. *Acta Crystallogr., Sect. E* **2008**, *64*, m928. (c) Li, Z.-Y.; Dai, J.-W.; Yue, S.-T. *Acta Crystallogr., Sect. E* **2009**, *65*, m775.

(15) Yao, Y.-L.; Che, Y.-X.; Zheng, J.-M. *Cryst. Growth Des.* **2008**, *8*, 2299.

(16) Wei, Y.-Q.; Yu, Y.-F.; Wu, K.-C. *Cryst. Growth Des.* **2008**, *8*, 2087.

(17) Ma, C.-L.; Li, Q.-L.; Zhang, R.-F. *J. Inorg. Organomet. Polym.* **2008**, *19*, 208.

(18) (a) Blatov, V. A.; Shevchenko, A. P. *TOPOS-Version 4.0 Professional* (*beta evaluation*); Samara State University: Samara, Russia, 2006. (b) Blatov, V. A.; Shevchenko, A. P.; Serezhkin, V. N. *J. Appl. Crystallogr.* **2000**, *33*, 1193.

(19) (a) Sheldrick, G. M. *SHELXS 97, Program for Crystal Structure Solution*; University of Göttingen: Göttingen Germany, 1997. (b) Sheldrick, G. M. *SHELXL 97, Program for Crystal Structure Refinement*; University of Göttingen: Göttingen, Germany, 1997. (c) Bruker, APEX II, SAINT; Bruker AXS Inc.: Madison, Wisconsin, USA, 2004.

(20) (a) Zhu, X.-D.; Lu, J.; Li, X.-J.; Gao, S.-Y.; Li, G.-L.; Xiao, F.-X.; Cao, R. *Cryst. Growth Des.* **2008**, *8*, 1897. (b) Yang, J.; Li, Q.; Yue, G.-D.; Cao, J.-J.; Li, G.-H.; Chen, J.-S. *Inorg. Chem.* **2006**, *45*, 2857.

(21) (a) Zhang, Z.-H.; Song, Y.; Okamura, T.; Hasegawa, Y.; Sun, W.-Y.; Ueyama, N. *Inorg. Chem.* **2006**, *45*, 2896. (b) Huang, Y.-G.; Wu, B.-L.; Yuan, D.-Q.; Xu, Y.-Q.; Jiang, F.-L.; Hong, M.-C. *Inorg. Chem.* **2007**, *46*, 1171.